Phase Behavior of Liquid Crystalline Polymer/Model Compound Mixtures: Theory and Experiment

Sukmin Lee,[†] Alfred G. Oertli,[‡] Mark A. Gannon,[§] Andrea J. Liu,[†,∥] Dale S. Pearson,[†,‡] Hans-Werner Schmidt,[‡] and Glenn H. Fredrickson*[,†,‡]

Department of Chemical and Nuclear Engineering, Materials Department, and Department of Physics, University of California, Santa Barbara, California 93106

Received November 1, 1993; Revised Manuscript Received March 28, 1994[⊕]

ABSTRACT: Mixtures of a nematic liquid crystalline polyester with three model compounds of different molecular weights and mesogenic character were investigated. Experimental phase diagrams were constructed of binary mixtures of the polymer with each of the three low molecular weight materials, using DSC and optical microscopy measurements. Theoretical phase diagrams were calculated to qualitatively resemble the experimental ones by adjusting one free parameter, namely, the Flory χ parameter. The agreement between theory and experiment is good, and the trends with χ are physically reasonable.

I. Introduction

Liquid crystalline polymers (LCPs) are materials that offer a unique combination of high tensile strength, unusual barrier properties, and excellent thermal stability.[1] As applications of these materials multiply, there will be increased emphasis on identifying effective processing methods and on blending or alloying with conventional thermoplastics. Indeed, there already exists a sizable literature on the thermodynamic properties and rheology of LCP–flexible polymer blends, and a few miscible systems have been identified.[2–6]

In this paper, we focus on the thermodynamic behavior of LCPs mixed with small molecule liquids.[7,8] The study of solution properties is useful mainly because LCPs are often processed or synthesized from solution. The presence of solvent may also lower the isotropic–nematic transition temperature so that the isotropic phase may be reached without polymer degradation. The phase behavior of LCP solutions depends on several factors, including chemical and conformational compatibility, and molecular weight.[7,9]

There have been several miscibility studies of side-chain liquid crystalline polymers with low molecular weight nematics.[10–14] Here, we focus on the phase behavior of main-chain liquid crystalline polymers in low molecular weight solvents of either nematic or isotropic character. Our approach is novel because it combines synthesis, experiment, and theory to study the influence of solvent molecular weight and mesogenic character on the phase behavior of LCP solutions. We use model compounds as solvents to minimize the effects of chemical incompatibility. This allows us to qualitatively compare experimental and theoretical phase diagrams to extract a single parameter, the Flory χ parameter, for each mixture. Since χ embodies interaction strengths, trends in χ yield insight into the origins of these interactions.

II. Experimental Section

A. Synthesis of LCP and Model Compounds. Materials. 4-(Hexyloxy)benzoic acid was prepared from 4-hydroxybenzoic acid (Aldrich) and 1-bromohexane (Aldrich) in ethanol and aqueous KOH. The corresponding acid chloride was obtained by stirring the pure (hexyloxy)benzoic acid (crystallized from ethanol) in excess thionyl chloride (Janssen). The product was obtained after evaporating excess thionyl chloride under reduced pressure and used without further purification. *tert*-Butylhydroquinone (Kodak) was recrystallized from toluene twice and then sublimed in vacuum at 100 °C. 4-*tert*-Butylcatechol (Aldrich) was purified by distillation under reduced pressure. 1,6-Bis(4-chlorobenzoyl)oxy]hexane was synthesized according to the literature.[15,16] Pyridine (Fisher) was dried over activated molecular sieves (Fisher, 4 Å); triethylamine (Fisher) was refluxed over CaH_2 (Aldrich) and distilled. THF was dried over potassium. All other chemicals were used as received. Commercially available Fascat 4100 catalyst (M & T Chemicals bv) was used without purification.

Instrumentation. Melting points and phase transitions were recorded on a Mettler TA 3000 apparatus, under nitrogen at a heating rate of 10 °C/min. The samples were also examined under a Nikon Optiphot-Pol 104 polarizing microscope equipped with a Mettler FP-82 hot stage. ^{1}H-NMR spectra were recorded using a Varian Gemini 200 spectrometer. IR spectra were recorded on a Perkin-Elmer 1600 FT-IR.

LC Polymer. The liquid crystalline polymer poly{oxy(*tert*-butyl-1,4-phenylene)oxycarbonyl-1,4-phenyleneoxy-1,6-hexanediyloxy-1,4-phenylenecarbonyl} (LCP) was synthesized by melt condensation of *tert*-butylhydroquinone and 1,6-hexanediylbis(4-oxybenzoyl chloride), according to a procedure in the literature.[16] Here we report that the same polymer can be synthesized via a melt transesterification reaction of 1,6-hexanediylbis(4-oxybenzoic acid) and *tert*-butylhydroquinone diacetate, thereby avoiding one step and the handling of highly reactive acid chloride. The reaction is carried out at temperatures between 200 and 240 °C with the addition of a Fascat 4100 transesterification catalyst. The presence of a liquid crystalline phase can be observed by monitoring the stir opalescence in the reaction mixture. An estimate of the degree of polymerization can be given by establishing the isotropization temperature of the polymer melt and comparing it to known transition temperatures of LCP samples with varying molecular weights.[16] ^{1}H-NMR ($CDCl_3$, ppm of TMS): 1.20–1.87 (m + s), 4.06 (t + t), 6.85–7.06 (m), 7.11 (s), 7.22 (s), 8.13–8.17 (m). IR (KBr, cm^{-1}): 2944, 2870, 1728, 1605.

Model Compounds. *tert*-Butylhydroquinone Di-4-(hexyloxy)benzoate (M1). A solution of 3.18 g (13.2 mmol) of 4-(hexyloxy)benzoyl chloride in 10 mL of THF was slowly added to an ice-cooled, stirred solution of 1.08 g (6.5 mmol) of *tert*-butylhydroquinone in 40 mL of dry pyridine and 2 mL (14 mmol) of triethylamine. After the cooling was removed (1 h), the solution was stirred for additional 20 h. The solution was then poured on acidified water. The precipitate was filtered off, redissolved in chloroform, and repeatedly extracted with 1 N hydrochloric acid and then with 1 N NaOH. After washing until neutral, the chloroform phase was dried over Na_2SO_4, filtered, and evaporated to dryness; the residue then crystallized from ethanol/chloroform. Yield: 2.9 g (78%). T_g: −8 °C. T_m: 70 °C. T_{N-I}: 93 °C.[17,18]

* To whom correspondence should be addressed.
† Department of Chemical and Nuclear Engineering.
‡ Materials Department.
§ Department of Physics.
∥ Permanent address: Department of Chemistry & Biochemistry, UCLA, Los Angeles, CA 90024.
⊕ Abstract published in *Advance ACS Abstracts*, May 15, 1994.

0024-9297/94/2227-3955$04.50/0

^{1}H-NMR ($CDCl_3$, ppm of TMS): 0.92 (6H, t), 1.28–1.62 (12H, m), 1.38 (9H, s), 1.83 (4H, m), 4.05 (4H, t), 6.99 (4H, d + d), 7.13 (2H, d broad), 7.24 (^{1}H, d + d), 8.17 (4H, d + d). IR (KBr, cm^{-1}): 2943, 2863, 1733, 1605.

1,6-Bis{(((((((4-(hexyloxy)phenylene)carbonyl)oxy)-2-*tert*-butylphenylene)oxy)carbonyl)phenylene)oxy}hexane (M2). The intermediate *tert*-butylhydroquinone 4-(n-hexyloxy)benzoate for the synthesis of M2 was prepared by slowly adding 3.25 g (13.5 mmol) of 4-(hexyloxy)benzoyl chloride in 30 mL of THF to a cooled solution of 10.8 g (65 mmol) of *tert*-butylhydroquinone and 6.3 g (62 mmol) of triethylamine in 60 mL of THF. After the addition was complete, the mixture was stirred for 48 h at room temperature. The triethylamine hydrochloride was filtered off, and the red solution was evaporated to dryness. The remaining oily residue was crystallized twice from ethanol. Yield: 3.5 g (70%). In such a procedure, we believe that only one isomer is formed. For steric reasons, we assume the ester group is formed predominantly at the hydroxy function which is in a meta position to the *tert*-butyl group. The NMR spectrum indicates that only one isomer is present. Thin layer chromatography (TLC) in different solvent combinations shows only one spot. T_m: 149 °C. ^{1}H-NMR ($CDCl_3$), ppm of TMS): 0.92 (3H, t), 1.28–1.92 (8H, m + 9H, s), 4.04 (2H, t), 4.85 (1H, s broad), 6.67 (1H, d), 6.91 (1H, dd), 6.97 (2H, d), 7.06 (1H, d), 8.14 (2H, d). IR (KBr, cm^{-1}): 3406, 2952, 2871, 1700, 1605.

A solution of 1.15 g (2.9 mmol) of 1,6-bis[(4-chlorobenzoyl)-oxy]hexane in 40 mL of chloroform was added to a cooled solution of 2.22 g (6 mmol) of the intermediate *tert*-butylhydroquinone 4-(*n*-hexyloxy)benzoate and 0.61 g (6 mmol) of triethylamine in 50 mL of chloroform. The solution was stirred at room temperature for 48 h. The mixture was concentrated to approximately 10 mL and precipitated in ethanol. The precipitate was filtered, washed with warm ethanol, and then reprecipitated from chloroform in cold ethanol. The dried product and LCP have identical IR spectra. The ^{1}H-NMR spectrum shows somewhat broadened line shapes. T_g: 20 °C. T_{N-I}: 142 °C. ^{1}H-NMR ($CDCl_3$, ppm of TMS): 0.92 (t), 1.20–1.90 (m + s), 4.05 (t + t), 6.85–7.06 (m), 7.13 (s), 7.24 (s), 8.10–8.25 (m). IR (KBr, cm^{-1}): 2943, 2871, 1728, 1605, 1251, 1159.

4-*tert*-Butylcatechol Di-4-(hexyloxy)benzoate (M3). A 5.56-g (23-mmol) quantity of 4-(hexyloxy)benzoyl chloride in 10 mL of THF was slowly added to a cooled solution of 1.90 h (11.4 mmol) of *tert*-butylchatechol in 50 mL of pyridine and 2.4 g (24 mmol) of triethylamine. After the addition was complete, the mixture was stirred at room temperature for 20 h. The red-brown solution was diluted with 200 mL of chloroform and extracted several times with 1 N HCl, then 1 N NaOH, and finally with water. The chloroform layer was dried over $MgSO_4$, then filtered, and evaporated to dryness, to yield a yellowish oil. The oil was separated from impurities over an alumina (Fisher) column in chloroform. The combined fractions were evaporated again to yield a water-clear liquid that crystallized on standing over several weeks. The melting point can only be observed in the first heating curve. Yield: 5.9 g (89%). T_g: −24 °C. T_m: 44 °C (first heating only). ^{1}H-NMR ($CDCl_3$, ppm of TMS): 0.90 (6H, t), 1.15–1.95 (16H, m + 9H, s) 3.98 (4H, t), 6.84 (4H, d + d), 7.24–7.38 (3H, m), 8.01 (4H, d + d). IR (KBr, cm^{-1}): 2943, 2868, 1745, 1600.

B. DSC Measurements and Polarization Microscopy. Sample Preparation. The different samples were prepared by dissolving the desired amounts (w/w) of polymer (LCP) and model compounds (M1, M2, M3) in chloroform. The solutions were cast on glass plates, and the chloroform was evaporated. The films were then dried in a vacuum oven at room temperature for 48 h.

DSC Measurements. Differential scanning calorimetry (DSC) was carried out using a Perkin-Elmer DSC-7. Indium (T_m: 156.4 °C) was used as a standard for calibration. All experiments were carried out under a constant flow of dry nitrogen. The sample weight was 18–20 mg. The heating rate was 10 °C/min. The data reported here were taken from second heating runs made after maintaining the samples at 20 °C above the isotropization temperature for 4 min and cooling with a dry ice/acetone mixture.

Polarization Microscopy. The mixtures were observed using a Nikon Optiphot Pol 104 polarizing microscope equipped with a Mettler hot stage (FP-82). Thin films having thicknesses of 50–70 μm were prepared by evaporing solutions of the mixtures in chloroform onto microscopy slides. The films were observed at a magnification of 100.

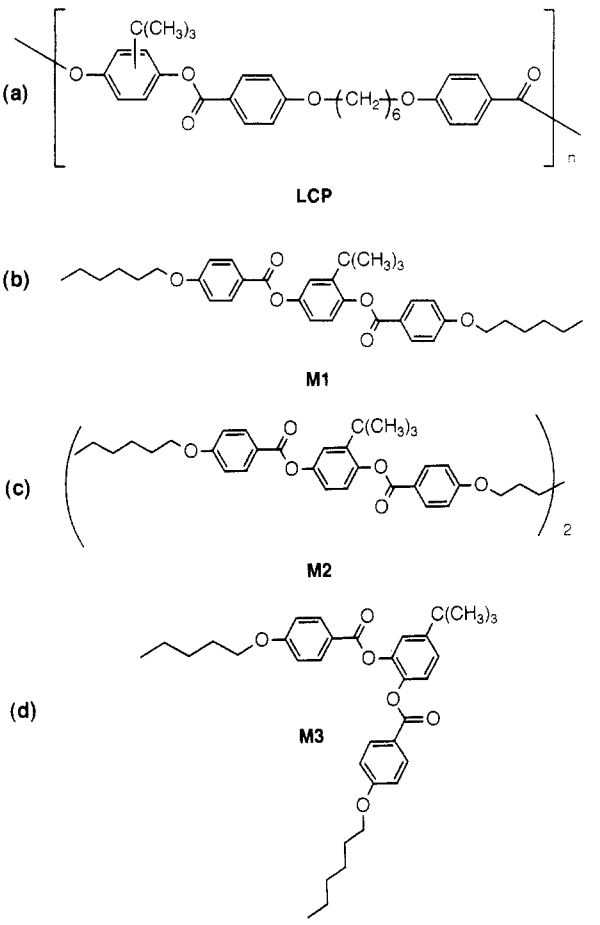

Figure 1. Chemical structures of the LCP and model compounds: (a) poly{oxy(*tert*-butyl-1,4-phenylene)oxy-1,6-bis[4-benzoyloxy]hexane} (LCP), constitutionally disordered; (b) *tert*-butylhydroquinone di-4-(hexyloxy)benzoate (M1); (c) 1,6-bis{(((((((4-(hexyloxy)phenylene)carbonyl)oxy)-2-*tert*-butylphenylene)oxy)carbonyl)phenylene)oxy}hexane (M2); (d) 4-*tert*-butylcatechol di-4-(hexyloxy)benzoate (M3), a constitutional isomer of M1.

III. Results and Discussion

A. Synthesis and Properties of Pure LCP and Model Compounds. The synthesis and characterization of the semiflexible liquid crystalline polyester poly{oxy-*tert*-butyl-1,4-phenylene)oxycarbonyl-1,4-phenyleneoxy-1,6-hexanediyloxy-1,4-phenylenecarbonyl} (LCP) (Figure 1a) has been described by Grizzuti et al.[16] For temperatures below $T_g \simeq 90$ °C, it forms a nematic glass. Above T_g, it is a nematic liquid over a wide temperature range, up to the isotropization temperature at $T_{N-I} \simeq 240$ °C.

The synthesis of the three different model compounds followed a modified procedure described for the synthesis of *tert*-butylhydroquinone di-4-(hexyloxy)benzoate, hereafter denoted as M1 (Figure 1b), and similar liquid crystalline compounds.[17,19] The syntheses of model compounds 1,6-bis{(((((((4-(hexyloxy)phenylene)carbonyl)-oxy)-2-*tert*-butylphenylene)oxy)carbonyl)phenylene)oxy}-hexane, denoted as M2 (Figure 1c), and 4-*tert*-butylcatechol di-4-(hexyloxy)benzoate, hereafter denoted as M3 (Figure 1d), were straightforward but required more care in purification. The ^{1}H-NMR spectra do not show any presence of significant impurities or constitutional isomers. Given the unavoidable polydispersity of the LCP, we expect that minor impurities in the model compounds (amounting to less than 1%) should not influence the results of the thermal and optical experiments.

Table 1. Molecular Weight and Thermal Properties of the Pure Liquid Crystalline Polymer (LCP) and Model Compounds (M1, M2, M3)

	M_w	T_g (°C)	T_m (°C)	T_{N-I} (°C)	ΔH_{N-I} (J/g)	ΔH_{N-I} (kJ/mol)
LCP	42300[a]	89		233	11.90	5.81[b]
M1	574	-8	70	94	3.65	2.10
M2	1062	20		142	8.09	8.60
M3	574	-24[c]	44[d]			

[a] M_n = 15 800, M_w/M_n = 2.7. Obtained by gel permeation chromatography (GPC), calibrated with polystyrene standards. See ref 11. [b] In units of kJ/mol of repeat units. [c] Upon cooling from the isotropic melt, the compound solidifies as an isotropic glass. [d] Only observed in the first heating curve.

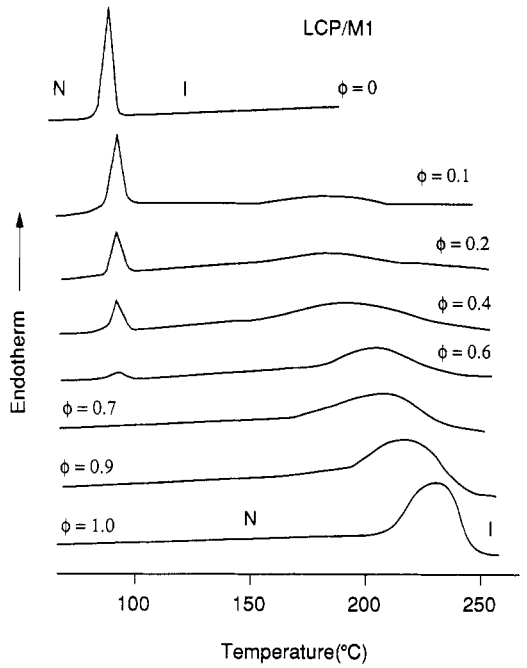

Figure 2. Typical DSC thermograms showing the transition temperatures of mixtures of LCP and model compound M1 at various compositions. Data reported are from second heating runs, taken at a heating rate of 10 °C/min, under nitrogen. Here, ϕ denotes the weight fraction of LCP, N denotes the nematic phase, and I denotes the isotropic phase.

Both analytical methods, IR as well as ^{1}H-NMR spectroscopy, yield similar spectra for the three model compounds and the polymer. In fact, the IR and the ^{1}H-NMR spectra of the LCP and M2 are almost identical. For the ^{1}H-NMR, the only significant difference in the spectra of the LCP and model compounds is that the latter contain a signal for the methyl end group at 0.92 ppm.

B. LCP/Model Compound Mixtures: Experimental Phase Diagrams. Properties of the pure LCP and model compounds are listed in Table 1. The glass transition, melting, and nematic–isotropic transition temperatures were obtained directly from DSC measurements. The change in enthalpy at the nematic–isotropic transition, ΔH_{N-I}, was obtained by integrating the DSC trace. Figure 2 contains typical DSC thermograms showing the nematic–isotropic transitions of LCP/M1 mixtures of various compositions. The nematic–isotropic transition at $T_{N-I} \simeq 89$ °C (see Table 1) of pure M1 is represented by a sharp peak characteristic of pure low molecular weight liquid crystals. We attribute the broadness of the corresponding signal at $T_{N-I} \simeq 233$ °C in pure LCP to its moderate polydispersity of 2.67, which is inevitably generated by the polycondensation reaction. Note that the *N–I* transition occurs at a higher temperature in the LCP than in M1. As the weight fraction of M1 in the mixtures increases, T_{N-I} decreases by 20–30 deg.

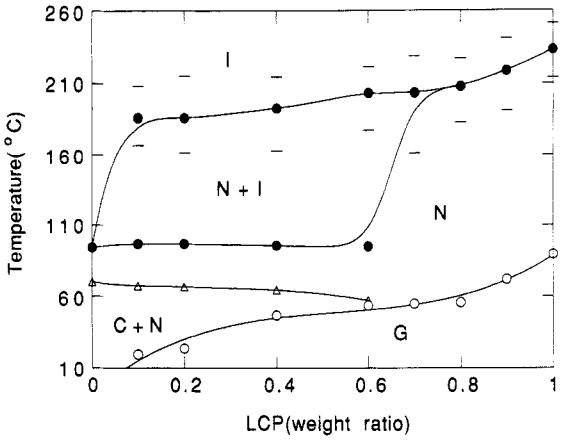

Figure 3. Phase diagram of LCP/M1 mixtures constructed from DSC analyses and optical microscopy of mixtures with different compositions. Isotropic, nematic, glassy, and crystalline phases are denoted by I, N, G, and C. Coexistence regions are labeled by plus signs; thus, the biphase is denoted by I + N. The lines above and below each data point indicate the width of the DSC peaks.

In the LCP/M1 mixtures with weight fractions of the LCP ranging from $\phi = 0.1$ to $\phi = 0.7$, two isotropic–nematic transition peaks appear in the DSC traces (see Figure 2). We interpret these as follows. At temperatures above the upper peak, the system is in a mixed, isotropic phase. Between the two peaks, the system lies in a biphase: it phase separates into a nematic phase rich in LCP coexisting with an isotropic phase rich in M1. Below the lower peak, the mixture is in a mixed, nematic phase. The temperatures marking the boundary of the biphase, marked by the upper and lower peaks, do not vary much in the range $0.1 \leq \phi \leq 0.6$. For $\phi \gtrsim 0.7$, only one point is shown on the phase diagram. This is because the biphase peak widths due to LCP polydispersity exceed the difference in their peak positions. The dependence of the width of the *N–I* transition peak on polydispersity in a pure liquid crystalline polymer has been reported.[20]

The phase diagram of LCP/M1 mixtures obtained from the DSC analysis is shown in Figure 3. The points on the diagrams are the locations of the peaks on the DSC traces. The width of each peak is indicated by lines above and below each point. The open circles represent T_g; at higher weight fractions of LCP, the mixture forms a glass rather than a crystal at low temperatures. The open triangles denote the transition from a mixed nematic phase to coexistence between a nematic phase rich in LCP and a crystalline phase rich in M1. Finally, the region containing the solid circles is interpreted, as discussed above, as a biphase region of isotropic–nematic coexistence.

To confirm the phase diagram in Figure 3, mixtures of selected composition were examined at various temperatures under a polarizing optical microscope. Figure 4 contains representative pictures of a ϕ = 0.4 LCP/M1 mixture. Figure 4a, taken at T = 70 °C, shows the mixture in a homogeneous nematic phase after annealing for 72 h. There is no noticeable change of morphology during that time. This suggests that the homogeneous nematic phase is indeed at equilibrium. Figure 4b, taken under crossed polarizers at T = 140 °C, shows the separation into coexisting isotropic and nematic phases. The dark domains are isotropic, while the bright areas are birefringent, and therefore nematic. Finally, Figure 4c, obtained using unpolarized light at T = 230 °C, demonstrates that the mixture forms a homogeneous isotropic phase at high temperatures.

The second mixture we studied was the LCP mixed with M2, whose molecules are approximately twice the size of

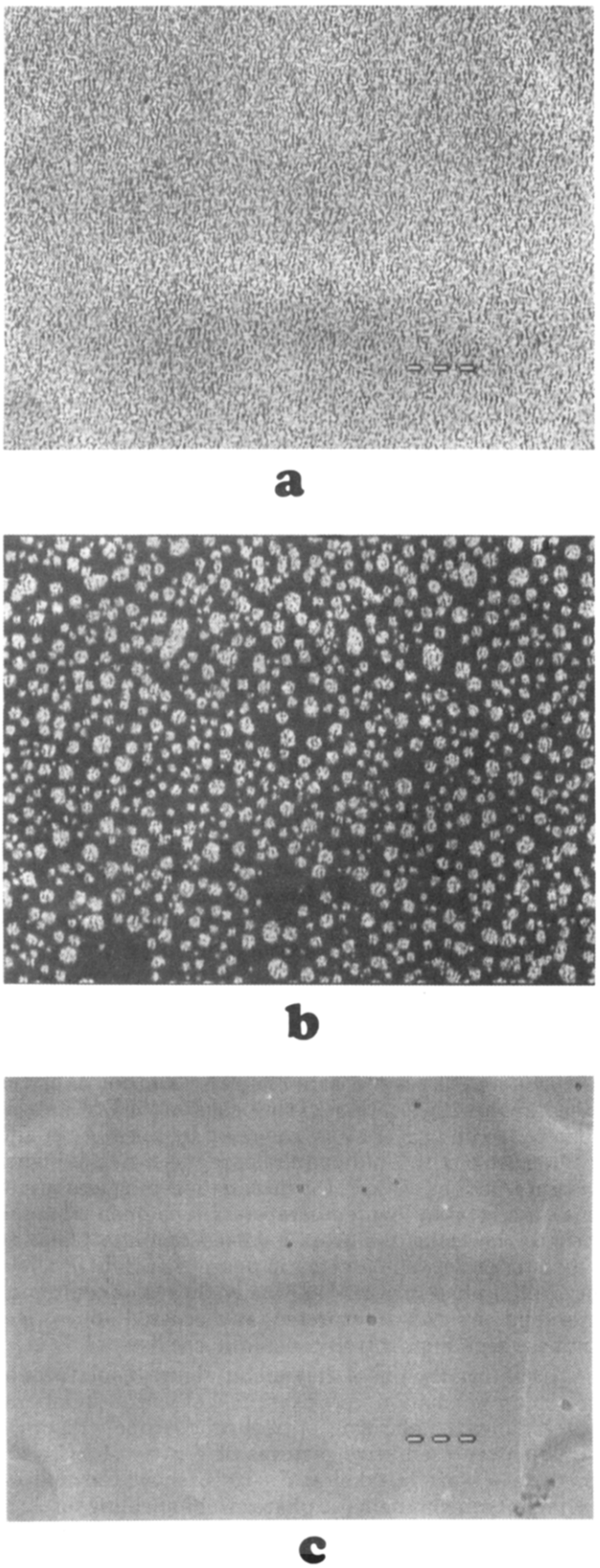

Figure 4. Representative pictures of a 0.4/0.6 LCP/M1 mixture at various temperatures, taken under an optical microscope at a magnification of 100. (a) A homogeneous nematic phase taken under crossed polarizers after annealing at 70 °C for 72 h. The dark streaks are nematic defect textures. (b) Coexisting domains of a nematic phase rich in LCP (bright) and an isotropic phase rich in M1 (dark) taken under crossed polarizers at 140 °C. (c) A homogeneous isotropic phase, taken under unpolarized light at 230 °C.

M1 molecules. The phase diagram for LCP/M2 mixtures is shown in Figure 5 and was constructed the same way

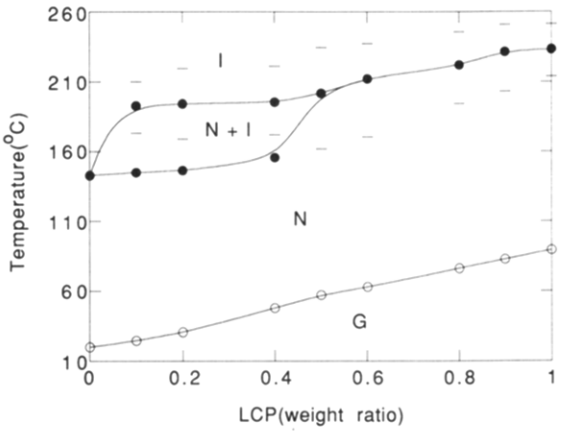

Figure 5. Phase diagram of LCP/M2 mixtures constructed from DSC and optical microscopy measurements. Isotropic, nematic, and glassy phases are denoted by I, N, and G. The lines above and below each data point indicate the width of the DSC peaks.

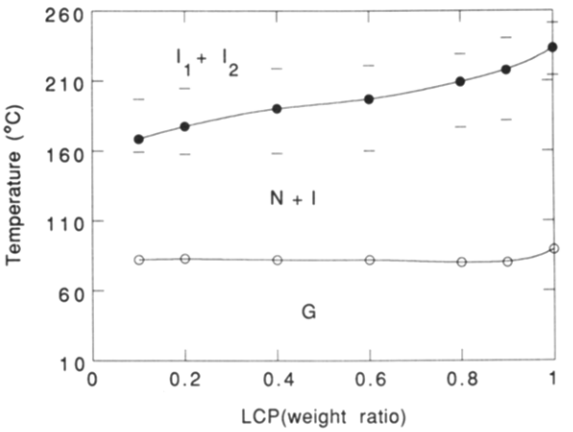

Figure 6. Phase diagram of LCP/M3 mixtures constructed from DSC analyses and optical microscopy. The lines above and below each data point indicate the width of the DSC peaks.

as the ones discussed above. It shows a close resemblance to Figure 3, except that no crystallization is observed in M2. Note that T_{N-I} is higher for pure M2 than pure M1, although still lower than for pure LCP. Thus, the biphase region, in which an isotropic phase rich in M2 coexists with a nematic phase rich in LCP, covers a smaller temperature range than the corresponding region on the LCP/M1 diagram. The experimental phase diagram for LCP/M2 blends, Figure 5, is plotted on the same temperature range as the one for LCP/M1 blends, Figure 3.

Note from Table 1 that the enthalpy change at the nematic–isotropic transition in weight units, ΔH_{N-I}, is highest for the LCP and lowest for M1. This suggests that the LCP/M2 mixture should be more miscible than the LCP/M1 mixture, as is observed.

The phase diagram for LCP/M3 mixtures is shown in Figure 6. The kinked model compound M3, a constitutional isomer of M1, is by nature not a liquid crystal. From Figure 6, we see that the addition of M3 does not lower the glass transition temperature T_g because the system phase separates into a glassy phase rich in LCP coexisting with an isotropic phase rich in M3. At intermediate temperatures, there is a biphase region where an isotropic phase rich in M3 coexists with a nematic phase rich in LCP. Above the biphase, the mixture separates into two coexisting isotropic phases, one rich in LCP and the other rich in M3. In contrast, mixtures of the LCP and M1, which is an isomer of M3, form a mixed isotropic phase at all compositions at temperatures above the biphase (see Figure 3). In principle, there should be an upper critical point for the LCP/M3 mixture at very high temperatures,

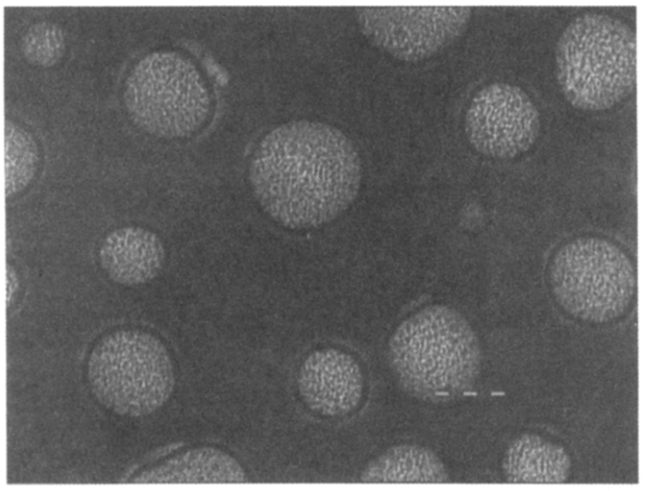

a

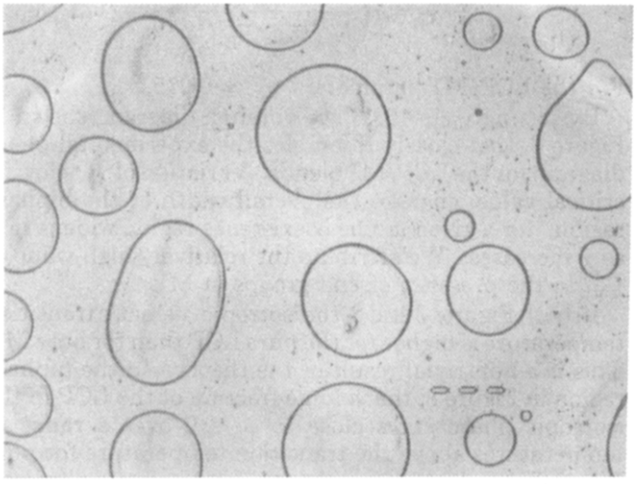

b

Figure 7. Representative pictures of LCP/M3 mixtures at different temperatures, taken under an optical microscope at a magnification of 100. (a) Nematic–isotropic phase coexistence shown at 120 °C under crossed polarizers. The bright domains are nematic and rich in LCP; the dark domains are isotropic and rich in M3. (b) Isotropic–isotropic phase coexistence at 230 °C. This was taken under unpolarized light.

above which the system forms a mixed isotropic phase. The critical point cannot be observed in this mixture, however, because M3 decomposes above T = 240 °C.

The compositions of the coexisting phases, or equivalently, the boundaries of the coexistence regions, lie too close to the pure components to be reliably determined from the DSC or optical microscopy measurements. For that reason, we have not drawn any phase boundaries between $\phi = 0$ and $\phi = 0.1$ in Figure 6.

Figure 7 contains pictures of a $\phi = 0.4$ LCP/M3 mixture, taken under a polarizing optical microscope. Figure 7a was taken at T = 120 °C, and confirms the nematic–isotropic phase separation shown in Figure 6 at that temperature and composition. Figure 7b confirms that two isotropic phases coexist at T = 230 °C. The size of the domains is of the order several hundred microns.

C. Theoretical Phase Diagrams. The theoretical aim of this work was to produce phase diagrams for model systems with parameters adjusted to mimic the molecules studied in the experiments. The starting point was a free energy functional for a blend of two polymers of arbitrary length and stiffness, derived by Liu and Fredrickson.[21] Brochard, Jouffroy, and Levinson[23] have used a similar free energy expression to study phase diagrams of side-chain liquid crystalline polymers. The advantage of main-chain liquid crystalline polymers is that the coefficients in the free energy, which Brochard and co-workers treated as unknown, phenomenological parameters, can be calculated from a microscopic model in terms of properties of the pure components.

The free energy functional was calculated from a microscopic model of a binary mixture (A + B) of wormlike chains, composed of cylindrical segments of length a_0 and volume a_0^3. The chains have contour lengths $N_A a_0$ and $N_B a_0$, and persistence lengths $\kappa_A a_0$ and $\kappa_B a_0$. Here, κ_A and κ_B are dimensionless bending rigidities that control the stiffness of the polymers. The volume fraction of species A is $\phi \equiv \phi_A$; the assumption of incompressibility constrains the volume fraction of species B to be $\phi_B = 1 - \phi$. Nematic order is parameterized by a tensor orientation density $\overleftrightarrow{S}$. Two interaction parameters are retained: a standard Flory parameter χ, which describes the tendency for demixing due to isotropic AA, AB, and BB interactions, and a Maier–Saupe parameter w, which describes the tendency for local segmental alignment due to anisotropic interactions. Note that to minimize the number of adjustable parameters, we assume in the present work that $w/4 = w_{AA} = w_{AB} = w_{BB}$.

The free energy functional has the form

$$\mathcal{F} = \mathcal{F}_{FH} + \mathcal{F}_{LdG} \tag{3.1}$$

where $\mathcal{F}$ is a free energy per monomer, in units of $k_B T$, and k_B is the Boltzmann constant. $\mathcal{F}_{FH}$ is the familiar Flory–Huggins free energy for a blend:

$$\mathcal{F}_{FH} = \frac{\phi}{N_A}\log\phi + \frac{1-\phi}{N_B}\log(1-\phi) + \chi\phi(1-\phi) \tag{3.2}$$

$\mathcal{F}_{LdG}$ is a Landau–de Gennes expansion in the nematic order parameter $\overleftrightarrow{S}$:

$$\mathcal{F}_{LdG} = \frac{1}{2}(B(\phi) - w)\mathrm{Tr}(\overleftrightarrow{S}^2) - \frac{1}{3}C_3(\phi)\mathrm{Tr}(\overleftrightarrow{S}^3) + \frac{1}{4}D_4(\phi)[\mathrm{Tr}(\overleftrightarrow{S}^2)]^2 \tag{3.3}$$

Usually, the coefficients B, C_3, and D_4 are treated as unknown phenomenological parameters. The advantage of Liu and Fredrickson's work is that they calculated these coefficients, within mean field theory, from the microscopic model described above. Thus, the free energy functional depends only on a small set of parameters, most of which can be determined from the pure components. These include the molecular weights and bending rigidities of the two pure components and the two free parameters, χ and w, that characterize the interactions. Explicit formulas for these coefficients are supplied in ref 16. Liu and Fredrickson also calculated square gradient terms in the free energy, but these do not affect bulk phase behavior.

Theoretical coexistence curves are obtained by analyzing the free energy for a blend. This amounts to finding common tangents to the free energy curves numerically. The details of the method used to find the common tangents will be presented elsewhere.[22]

Although the model compounds M1, M2, and M3 were synthesized to be chemically similar to the LCP, they are not identical, so the isotropic interaction parameter χ

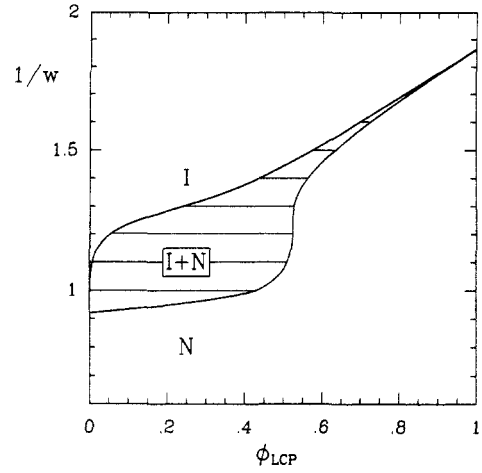

Figure 8. Theoretical LCP/M1 phase diagram. The LCP is modeled by $N_A = 200$, $\kappa_A = 20$ and M1 is modeled by $N_B = 10$, $\kappa_B = 20$; see text. This diagram should be compared to the experimental phase diagram in Figure 3. The Flory χ parameter is $\chi = 0.06$.

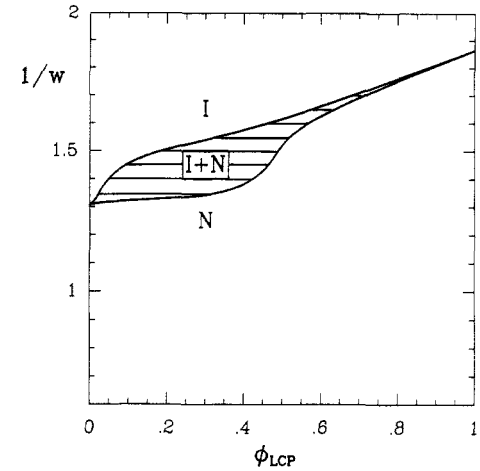

Figure 9. Theoretical LCP/M2 phase diagram. The LCP and M2 are modeled by $N_A = 200$, $\kappa_A = 20$ and $N_B = 20$, $\kappa_B = 20$; see text. This diagram should be compared to the experimental phase diagram in Figure 5. We chose $\chi = 0.035$ for this plot.

should be nonzero. No critical points are observed in the experimental phase diagrams, however, so χ appears to vary slowly with temperature (at fixed composition) over the temperature range studied. For simplicity, we assume that χ does not vary with temperature.

On the other hand, isotropic–nematic transitions are observed, so the anisotropic interaction parameter w must change over the temperature range covered in the experiments. We assume that w has an approximate temperature dependence of the form

$$w(T) \approx w_0 + \frac{w_T}{T} \tag{3.4}$$

and we subsequently use $1/w$ as a "temperature" scale. If we take eq 3.4 literally and use the isotropic–nematic transition temperatures for pure M1 and M2 to determine w_0 and w_T, the theoretically estimated transition temperature for the pure LCP is $T_{N\text{-}I} = 190$ °C. This is lower than the experimentally determined $T_{N\text{-}I} = 233 \pm 20$ °C. Since we cannot unambiguously determine the functional dependence of w on T from the experiments, we cannot draw the theoretical phase diagrams on a true temperature scale. Nevertheless, it will soon be apparent that remarkable qualitative agreement of theory and experiment results from using $1/w$ in place of T. In all of the theoretical phase diagrams, we plot ϕ, always defined as the volume fraction of the LCP, on the horizontal axis and $1/w$ on the vertical axis. (Note that the experimental phase diagrams were plotted as a function of *weight* fraction of the LCP rather than volume fraction.) For each mixture, the Flory parameter χ is adjusted to make the theoretical phase diagram resemble its experimental counterpart.

The first theoretical phase diagram, Figure 8, is meant to correspond to the experimental phase diagram for the LCP/M1 mixtures, Figure 3. We have chosen $N_A = 200$ and $N_B = 10$ to model the LCP and M1, respectively. This ratio of molecular weights, 20 to 1, is similar to the 24:1 ratio of molecular weights in the mixtures studied in the experiments. The choice of the bending rigidity of M1 is somewhat arbitrary; we have used $\kappa_B = 20$. This corresponds to a persistence length of $\kappa_B a_0 = 20a_0$, which is twice the contour length $N_B a_0$. This ensures that M1 molecules are quite rigid. Since the chemical structure of the LCP is similar to M1, we choose $\kappa_A = \kappa_B = 20$. Finally, we can use the experimental observations to establish an upper bound on χ. Figure 3 does not show isotropic–isotropic phase separation, so χ, which favors phase separation, cannot exceed its critical value

$$\chi_c = \frac{1}{2}\left(\frac{1}{N_A^{1/2}} + \frac{1}{N_B^{1/2}}\right)^2 \tag{3.5}$$

For the LCP/M1 parameters, $\chi_c \simeq 0.075$.

By setting $\chi_{M1} = 0.06$, we obtain a diagram, shown in Figure 8, that closely resembles the experimental phase diagram for the LCP/M1 blends. Variation of χ, below its critical value, changes the overall width of the biphase region: for a given w, the coexistence region widens in ϕ as χ increases. We attribute the relatively high value of χ_{M1} to the presence of end groups in M1.

In both Figures 3 and 8, the isotropic–nematic transition temperature is higher for the pure LCP than for pure M1. This is a nontrivial result of the theory. In the biphase region in Figure 8, the volume fraction of the LCP in the isotropic phase stays close to $\phi = 0$ over a range of temperatures above the transition temperature for pure M1. The volume fraction of the nematic phase at coexistence also remains nearly constant over the same temperature range. This gives the lower part of the biphase area its nearly rectangular shape, seen also in the experimental diagram in Figure 3.

Note that in Figure 8, there is a narrow region of coexistence between an isotropic phase and a nematic phase, both at high LCP volume fraction, with the nematic phase slightly richer in LCP. This is not shown in the experimental phase diagram, because the narrow neck is subsumbed by the smearing of $T_{N\text{-}I}$ due to polydispersity of the LCP.

The second theoretical diagram, Figure 9, represents the same system as the second experimental diagram, Figure 5: namely, LCP/M2 mixtures. The molecular parameters used to model these mixtures are almost the same as for the LCP/M1 blends. For the LCP, we use $N_A = 200$ and $\kappa_A = 20$, as before. Again, we choose $\kappa_B = 20$. The only parameter changed is the degree of polymerization for the smaller molecules. Since M2 is roughly twice the size of M1, we choose $N_B = 20$.

The critical value of χ for the LCP/M2 system is $\chi_c \simeq 0.043$, lower than χ_c for the LCP/M1 system. The theoretical diagram made with $\chi_{M2} = 0.035$, shown in Figure 9, is quite similar to the experimental diagram for LCP/M2 blends, shown in Figure 5. Note that χ_{M2}, used for LCP/M2 mixtures, is lower than χ_{M1} used for LCP/M1 mixtures. If chemical differences between the different molecules are attributed to end groups, as discussed above,

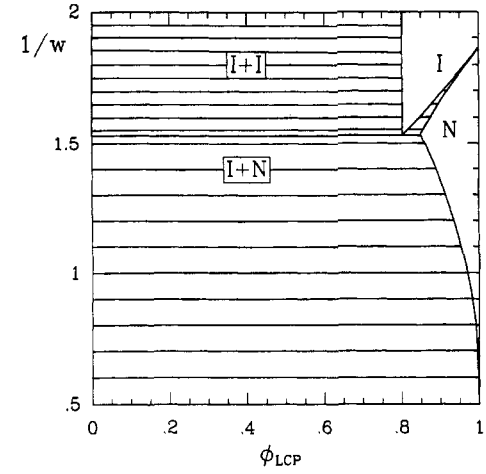

Figure 10. Theoretical LCP/M3 phase diagram. The model parameters are $N_A = 200$, $\kappa_A = 20$ and $N_B = 10$, $\kappa_B = 0$; see text. This plot should be compared to the experimental phase diagram in Figure 6. We fixed $\chi = 0.133$ in this figure. The composition of the LCP-poor isotropic phase is so low that it appears to be zero in the plot.

then a lower χ is indeed expected for LCP/M2 mixtures, because M2 is longer than M1.

The theoretical diagram resembles the experimental diagram in several important aspects. We find that the N–I transition temperature for pure M2 is higher than for pure M1 and lower than for the pure LCP, as seen in the experiments. Thus, the temperature range spanned by the biphase is smaller for the LCP/M2 blends than for the LCP/M1 blends. All of the theoretical phase diagrams are plotted over the same overall range of $1/w$, just as all of the experimental diagrams are plotted over the same temperature range.

The volume fraction of LCP in the isotropic phase coexisting with a nematic phase on the LCP/M2 phase diagram does not stay as close to $\phi = 0$ as in the LCP/M1 phase diagram. This is because the lengths of the two types of molecules are more similar in the LCP/M2 system. Also, the right (higher ϕ) boundary of the widened part of the coexistence region, which corresponds to the composition of the nematic phase, is less steep in the LCP/M2 diagram (Figure 9) than in the LCP/M1 diagram (Figure 8). This makes the biphase region on the LCP/M2 diagram less rectangular than the corresponding region on the LCP/M1 diagram.

The third theoretical diagram, Figure 10, is intended to represent blends of the LCP with M3, the kinked model compound. The kink frustrates nematic ordering of M3 molecules. In the context of the Liu–Fredrickson theory, the kinked molecules should have the same molecular weight as the M1 molecules, so we use $N_B = 10$. The most important characteristic of M3 molecules is their inability to form nematic phases, at least in the temperature range studied. To emulate this property, the persistence length is set to zero ($\kappa_B = 0$). The value of w at which a melt of molecules of zero persistence length goes nematic is infinite, which implies that such a melt cannot form a nematic phase at nonzero temperatures.

The experimental phase diagram for LCP/M3 mixtures, Figure 6, is strikingly different from the diagrams for the other two types of blends studied. Because the kinked molecules cannot form a nematic phase, there is no lower boundary to the isotropic–nematic coexistence region with a nematic region below, as there is in the diagrams for the other blends.

Another important difference is the broad isotropic–isotropic coexistence region experimentally observed in the LCP/M3 blends at high temperatures. In the other two types of blends, there is a single mixed isotropic phase at high temperatures. The existence of isotropic–isotropic phase separation implies a large χ parameter between the LCP and M3. In terms of the Flory theory, this requires an interaction parameter well above the critical value $\chi_c \simeq 0.0749$. The kinked molecule M3 is an isomer of M1, so it may seem that the value of χ should be the same for LCP/M1 and LCP/M3 mixtures. We attribute the larger value of χ_{M3} to a large entropic contribution to χ due to the difficulty of packing M3 with LCP.

In Figure 10, we chose $\chi_{M3} = 0.133$. This choice yields coexistence between isotropic phases at $\phi \simeq 2.498 \times 10^{-5}$ and $\phi \simeq 0.8019$. In the experiments, the composition of the LCP-rich isotropic phase exceeds $\phi = 0.9$, but the choice $\chi = 0.133$ is large enough that the phase behavior produced by the theoretical model (Figure 10) may be considered similar to that observed in the experiments (Figure 6). The value of χ required to produce a diagram more like the experimental diagram would have to be even higher. Even at $\chi = 0.133$, the composition of the LCP-poor isotropic phase in coexistence is extremely close to $\phi = 0$. Experimentally, the composition of the LCP-poor isotropic phase lies between $\phi = 0$ and $\phi = 0.1$.

The theoretical diagram has a narrow isotropic–nematic coexistence "neck" between $\phi \simeq 0.8019$ and $1/w \simeq 1.53$ and $\phi = 1$ and $1/w \simeq 1.86$, the transition value for pure LCP. It resembles the necks predicted in Figures 8 and 9 for LCP/M1 and LCP/M2 mixtures near $\phi = 1$. Again, it is not seen in the experimental diagram because it is obscured by the spread in the N–I transition temperature due to polydispersity of the LCP.

At $1/w \simeq 1.53$, a horizontal line separates isotropic–isotropic coexistence from isotropic–nematic coexistence below. On the experimental phase diagram, the line separating the two regions is not horizontal. This effect could be due to polydispersity in the LCP, which would affect blends at higher volume fractions of LCP more than those at lower volume fractions.

On the theoretical diagram, there is a narrow region near $\phi = 1$ below the "neck" in which a mixed nematic phase is stable. This region is narrower for higher values of χ. On the experimental diagram, such a region is not shown. A sample was prepared at $\phi = 0.95$ and was observed under the microscope after annealing for 4 h. The system appeared to be in a mixed nematic phase, but this could also be due to slow phase separation kinetics, since the polymer is highly viscous.

The good qualitative agreement between the theoretical and experimental phase diagrams for the LCP/M3 system shows that the phase behavior is relatively insensitive to details of the shapes of the molecules. Note that M3 was not modeled as a kinked molecule. Rather, we have approximated it as a flexible chain molecule. We have, however, captured what is apparently the most important property of M3—its inability to form a nematic phase.

IV. Conclusions

In this study, we have combined synthesis, experiment, and theory to systematically examine the phase behavior of binary blends of a liquid crystalline polymer with three model compounds of varying molecular weight and mesogenic character. The model compounds M1 and M2 are thermotropic liquid crystals; M2 has twice the molecular weight of M1. The third model compound, M3, is a non-liquid-crystalline isomer of M1. As expected, we find that LCP/M2 mixtures are more miscible than LCP/M1 mixtures, because M2 is more similar in length to the LCP. Similarly, LCP/M1 mixtures are more miscible than LCP/

M3 mixtures, because M1 is more similar to the LCP in its mesogenic nature.

Using DSC and optical microscopy measurements, we have constructed experimental phase diagrams in composition and temperature for the three mixtures. By adjusting only one free parameter in a free energy functional obtained earlier,[21] we have calculated theoretical phase diagrams in excellent qualitative agreement with the experimental ones. The single free parameter is the Flory χ parameter, which characterizes the strnegth of isotropic interactions among segments. In order to obtain a good match between theory and experiment, we find that χ should be smallest for LCP/M2 mixtures and largest for LCP/M3 mixtures. This trend is physically reasonable; if we attribute the chemical difference between LCP and M1 or LCP and M2 to end groups, χ should decrease as the molecular weight of the model compound increases. We attribute the large χ observed in the LCP/M3 mixtures to an entropic contribution that arises from packing molecules of very different shapes. Evidently, this entropic contribution is much larger than the contribution to χ due to end groups.

In summary, we have used a simple model of wormlike chains to approximate the shapes of the LCP and model compounds. This is quite a caricature, especially for M3, which is a kinked molecule. In spite of the crudity of the model, however, we are able to compare theoretical and experimental phase diagrams to obtain physically reasonable estimates of interaction strengths in systems where both phase separation and isotropic–nematic transitions can occur. This success demonstrates that the general approach should be fruitful for semiflexible polymer solutions and blends.

Acknowledgment. We thank Pat Mather for helpful discussions. This work was supported by the National Science Foundation, through the Materials Research Laboratory at the University of California, Santa Barbara, under Grant No. DMR-9123048. A.G.O. and M.A.G., respectively, acknowledge the support of the Jubiläumsstiftung der CIBA-GEIGY AG, Basel, Switzerland, and the U. S. Department of Education, through a Condensed Matter Fellowship.

References and Notes

(1) National Research Council. *Liquid Crystalline Polymers*; Report of the Committee on Liquid Crystalline Polymers, NMAB-453; National Academy Press: Washington, DC, 1990.
(2) Dutta, D.; Fruitwala, H.; Kohli, A.; Weiss, R. A. *Polym. Eng. Sci.* **1990**, *30*, 1005.
(3) Sukhadia, A. M.; Done, D.; Baird, D. G. *Polym. Eng. Sci.* **1990**, *30*, 519.
(4) Silverstein, M. S.; Hiltner, A.; Baer, E. *J. Appl. Polym. Sci.* **1991**, *43*, 157.
(5) Perkins, E. G.; Marcelli, A. M.; Frerking, H. W. *J. Appl. Polym. Sci.* **1991**, *43*, 329.
(6) Kim, W. N.; Denn, M. M. *J. Rheol.* **1992**, *36*, 1477.
(7) Ciferri, A., Ed. *Liquid Crystallinity in Polymers*; VCH Publishers, Inc.: New York, 1991.
(8) Donald, A. M.; Windle, A. H. *Liquid Crystalline Polymers*; Cambridge University Press: New York, 1992.
(9) Ratto, J. A.; Volino, F.; Blumstein, R. B. *Macromolecules* **1991**, *24*, 2862.
(10) Nyitrai, K.; Cser, F.; Lengyel, M.; Seyfried, E.; Hardy, G. *Eur. Polym. J.* **1977**, *13*, 673.
(11) Ringsdorf, H.; Schmidt, H.-W.; Schneller, A. *Makromol. Chem. Rapid Commun.* **1982**, *3*, 745.
(12) Casagrande, C.; Veyssié, M.; Weill, C.; Finkelmann, H. *J. Phys. Lett.* **1982**, *43*, L671.
(13) Benthack-Thoms, H.; Finkelmann, H. *Makromol. Chem.* **1985**, *186*, 1895.
(14) McArdle, C. G., Ed. *Side Chain Liquid Crystal Polymers*; Chapman and Hall: New York, 1989; Chapter 6 and references therein.
(15) Griffin, A. C.; Havens, S. J. *J. Polym. Sci.* **1981**, *19*, 951.
(16) Mather, P.; Grizzuti, N.; Heffner, G.; Mather, P.; Ricker, M.; Rochefort, W. E.; Seitz, M.; Schmidt, H.-W.; Pearson, D. S. Preprint.
(17) Wedler, W.; Demus, D.; Zaschke, H.; Mohr, K.; Schafer, W.; Weissflog, W. *J. Mater. Chem.* **1991**, *1*, 347.
(18) Weissflog, W.; Schlick, R.; Demus, D. *Z. Chem.* **1981**, *21*, 452.
(19) Dewar, J. S.; Griffin, A. C. *J. Am. Chem. Soc.* **1975**, *97*, 6662.
(20) Laus, M.; Angeloni, A. S.; Galli, G.; Chiellini, E. *Macromolecules* **1992**, *25*, 5901.
(21) Liu, A. J.; Fredrickson, G. H. *Macromolecules* **1993**, *26*, 2817.
(22) Gannon, M. A.; Liu, A. J.; Fredrickson, G. H. To be published.
(23) Brochard, F.; Jouffroy, J.; Levinson, P. *J. Phys. (France)* **1984**, *45*, 1125.